Voltage and Cosubstrate Dependence of the Na-HCO_3 Cotransporter Kinetics in Renal Proximal Tubule Cells

Eitan Gross and Ulrich Hopfer
Department of Physiology and Biophysics, Case Western Reserve University, Cleveland, Ohio 44106-4970 USA

ABSTRACT The voltage dependence of the kinetics of the sodium bicarbonate cotransporter was studied in proximal tubule cells. This electrogenic cotransporter transports one Na^+, three HCO_3^-, and two negative charges. Cells were grown to confluence on a permeable support, mounted on a Ussing-type chamber, and permeabilized apically to small monovalent ions with amphotericin B. The steady-state, di-nitro-stilbene-di-sulfonate-sensitive current was shown to be sodium and bicarbonate dependent and therefore was taken as flux through the cotransporter. Voltage-current relations were measured as a function of Na^+ and HCO_3^- concentrations between −160 and +160 mV under zero-trans and symmetrical conditions. The kinetics could be described by a Michaelis-Menten behavior with a Hill coefficient of 3 for HCO_3^- and 1 for Na^+. The data were fitted to six-state ordered binding models without restrictions with respect to the rate-limiting step. All ordered models could quantitatively account for the observed current-voltage relationships and the transinhibition by high bicarbonate concentration. The models indicate that 1) the unloaded transporter carries a positive charge; 2) the binding of cytosolic bicarbonate to the transporter "senses" 12% of the electric field in the membrane, whereas its translocation across the membrane "senses" 88% of the field; 3) the binding of Na^+ to the cotransporter is voltage independent.

INTRODUCTION

The electrogenic Na-HCO_3 cotransporter comprises the main exit pathway for HCO_3^- across the basolateral membrane in the proximal tubule (Yoshitomi and Fromter, 1984; Burckhardt et al., 1984; Yoshitomi et al., 1985; Biagi, 1985; Sasaki et al., 1985; Alpern, 1985; Jentsch et al., 1985, 1986; Biagi and Sohtell, 1986; Alpern and Chambers, 1986; Jentsch et al., 1986; Akiba et al., 1986; Soleimani et al., 1987; Lopes et al., 1987). Cotransporter activity results in the net reabsorption of HCO_3^- from the tubule lumen to the blood. Both Na^+ and HCO_3^- are cotransported across the basolateral membrane of the proximal tubular cell against their respective concentration gradients. The driving force for the process is the (inside negative) membrane potential. Thus any change in membrane potential will also affect the turnover of the cotransporter. Thermodynamically, the electrical potential difference is like a driving force fully exchangeable with an equivalent chemical potential difference. This is not necessarily so for the rates of cotransport. The effectiveness of the membrane potential as a driving force depends on molecular details, such as which steps in the transport cycle are voltage dependent (binding or dissociation of the substrates, translocation of the loaded and unloaded carrier), whether charge transport is by the loaded or unloaded form of the carrier, and whether the rate-limiting step is voltage sensitive. The data obtained from transport studies, in which the cotransporter is driven by either membrane potential or chemical gradients, complement each other. Obviously, any realistic model of a given cotransporter should be able to describe the results obtained under the two sets of conditions.

The whole-cell recording technique has been used to study the activity of the Na-HCO_3 cotransporter and has provided direct evidence for the potential dependence of this cotransporter. Two experimental systems have been used to measure electrogenic properties of cotransporter activity. In one case whole-cell recordings from dissected tubules were used to measure cotransporter activity in the native state (Boron and Boulpaep, 1983; Yoshitomi et al., 1985; Coppola and Frömter, 1994). A quantitative study of cotransporter activity with the whole-cell model is complicated by its inability to vary intracellular substrate concentrations, and hence its inability to vary the thermodynamic driving force. More recently, activity of the cotransporter from the rabbit proximal tubular clone (Burckhardt et al., 1994) and the salamander kidney clone (Romero et al., 1997) expressed in *Xenopus* oocytes has been measured. This is an exogenous expression system that lacks the native intracellular environment and potential regulatory accessory proteins that may be important determinants of the kinetic properties of the cotransporter in the native state. Nevertheless, both types of studies have provided direct evidence for the rheogenicity of the transport cycle and indicated the extent to which its turnover is dictated by the membrane potential.

In a previous study, we measured the stoichiometry of the Na-HCO_3 cotransporter in a proximal tubular cell line and found it to be 3 HCO_3^-:1 Na^+ (Gross and Hopfer, 1996). The Na-HCO_3 cotransporter is expressed endogenously in this cell line. In the present study, we used the same cell line to study the kinetic properties of the cotransporter. We measured the cotransporter's current-voltage relationships under symmetrical and zero-trans conditions. Under symmetrical conditions, i.e., identical solutions on either side of

Received for publication 8 December 1997 and in final form 8 May 1998.
Address reprint requests to Dr. Eitan Gross, Department of Physiology and Biophysics, Case Western Reserve University, 10900 Euclid Ave., Cleveland, OH 44106-4970. Tel.: 216-368-4469; Fax: 216-368-3952; E-mail: ezg@po.cwru.edu.

0006-3495/98/08/810/15 $2.00

the monolayer, the membrane potential is the only driving force for the cotransport, whereas under zero-trans conditions both the concentration gradient and the electrical potential drive the flux through the cotransporter. We used a proximal tubular cell line that can be grown on a permeable support to form a polarized cell monolayer. The monolayer exhibits high electrical resistance and can thus be studied in a Ussing chamber by electrophysiological techniques. By selective permeabilization of the apical membrane, with an appropriate agent (e.g., amphotericin B), one can control, maintain, and manipulate the intracellular concentrations of the cotransporter's substrates, through free diffusion exchange between the apical perfusion solution and the cell cytoplasm. Thus the technique allows one to control the thermodynamic driving force acting on the cotransporter, thereby overcoming some of the limitations encountered in isotope influx experiments. The ability to control and modify the intracellular substrate concentrations as well as the membrane potential allows one to describe the free energy of the system and, therefore, to analyze the potential dependence of the cotransport mechanism. The experimental data in this study were fitted to mathematical transport models. The models could account for the global electrical properties of the cotransporter. A single set of numerical rate constants was found to account for the cotransporter's current-voltage relationships under various experimental conditions. From these numerical values, one can identify which steps in the transport cycle are rate-limiting under a defined set of conditions, and which steps are potential sensitive.

MATERIALS AND METHODS

Cell culture

Experiments were carried out with the rat proximal tubular cell line SKPT-0193 C1.2 (Woost et al., 1996). The line is derived from microdissected primary cultures of the S1 region of the proximal tubule. Passages 50–70 were used for the reported experiments. Cells were grown on collagen-coated (20% bovine hoof collagen in 60% ethanol) Millicell-CM filters (area = 0.6 cm^2) in a 1:1 mixture of Dulbecco's modified essential medium and Ham's F12, supplemented with 15 mM HEPES, 1.2 mg/ml $NaHCO_3$, 5 μg/ml insulin, 5 μg/ml transferrin, 5 ng/ml epithelial growth factor, 4 μg/ml dexamethasone, and 10% fetal bovine serum. Typically, 3×10^5 cells were seeded and grown to confluence in 5 days. Light microscopy showed a "cobblestone" appearance that is typical of the morphology of epithelial cells.

Electrophysiology

Confluent SKPT-0193 C1.2 cells have a low basal monolayer conductance of 0.5–1 mS/cm^2, indicating the poor ion permeability of tight junctions. This low baseline conductance allows the detection of electrical signals from cellular transporters that make only small contributions to the overall monolayer conductance. Filters with cells were mounted horizontally in a Ussing-type chamber (Analytical Bioinstrumentation, Cleveland, OH) equipped with voltage and current electrodes. Only cell monolayers with an initial conductance of 1 mS/cm^2 or less were used in the experiments described here. Electrophysiological measurements were made with a voltage-clamp module (model 558-C-5; Bioengineering, University of Iowa, IA) controlled by an IBM PC via the DATAQ software package (Dataq Instruments, Akron, OH). Current and voltage were recorded with a strip-chart recorder and in parallel through an A/D converter on a microcomputer. The apical and basolateral compartments of the Ussing chamber have a volume of 0.5 ml each. The cells are perfused separately on each side of the monolayer with a peristaltic pump at a rate of ~2 ml/min. The chamber and all solutions were maintained in a heated incubator allowing control of CO_2 pressure (pCO_2) and temperature.

For experiments that were carried out under zero-trans conditions, apical solutions contained (in mM) 2.5 Ca gluconate, 1.1 Mg gluconate, 100.0 HEPES, 25.0 D-glucose, 80 *N*-methyl-D-glucamine (NMDG), and 0.1% bovine serum albumin (BSA). Basolateral solutions contained (in mM) 2.5 Ca gluconate, 1.1 Mg gluconate, 100.0 MES, 25.0 D-glucose, 80 NMDG, and 0.1% BSA. For experiments in which the kinetics of the cotransporter to Na^+ were studied by varying the apical Na^+ concentration, $[Na^+]_{ap}$, at a fixed $[HCO_3^-]_{ap}$, NMDG was replaced with Na gluconate, in an isoosmotic manner. The pH of the apical and basolateral solutions was adjusted to 7.5 and 6.0, respectively, with acetic acid. Bicarbonate concentration was determined from the Henderson-Hasselbalch relation, $[HCO_3^-] = 3 \times 10^{-5} \cdot pCO_2 \cdot 10^{(pH\ -6.1)}$ (pCO_2 is given in mm Hg), by adjusting the CO_2 pressure to the appropriate value. From the above equation it can be seen that the difference of 1.5 pH units between the apical and basolateral solutions results in a 31-fold ($=10^{1.5}$) higher HCO_3^- concentration in the apical solution compared to that in the basolateral solution, at any CO_2 pressure.

For experiments carried out under symmetrical conditions, apical and basolateral solutions contained (in mM) 2.5 Ca gluconate, 1.1 Mg gluconate, 100.0 HEPES, 25.0 D-glucose, 80 NMDG, and 0.1% BSA. In experiments in which the concentration of Na^+ was varied, NMDG was replaced with Na gluconate in an isoosmotic manner. The pH of the apical and basolateral solutions was adjusted to 7.5 with acetic acid. The bicarbonate concentration was set and determined from the Henderson-Hasselbalch relation, by adjusting the CO_2 pressure to the appropriate value, as described above.

All solutions were first adjusted for pH with acetic acid and then preequilibrated with CO_2 at the appropriate pCO_2 for 1 h. The pH of the solutions was measured and adjusted again before the beginning of the experiment and was measured once more at the end of each experiment. The solutions were maintained at the appropriate pCO_2 throughout the entire experiment, and the pH was found to change by less than 0.1. Experiments were carried out at 37°C. CO_2 pressure was continuously monitored with a CO_2 monitor (Puritan-Bennett, Los Angeles, CA).

To determine the cotransporter's current-voltage (*I-V*) relation, cell monolayers were permeabilized with 10 μM apical amphotericin B as described previously (Gross and Hopfer, 1996). After I_{sc} had leveled off, an *I-V* relation was obtained by running a custom program that steps a voltage between −160 and +160 mV in 20-mV increments. The basolateral compartment was then perfused with 1 mM 4,4′-dinitrostilbene-2,2′-disulfonic acid (DNDS) for 10 min to ensure full equilibration of DNDS with the cotransporter (see also Fig. 2), and a second *I-V* relation was obtained. The difference current (ΔI) was plotted against voltage to obtain the voltage dependence of the cotransporter. The fit of the data to the Michaelis-Menten and the Hill equations (i.e., Figs. 4 *B* and 7 *B*) revealed that although the I_{max} values obtained from different cells were different from each other, there was no statistical difference between the $K_{0.5}$ values obtained from these cell monolayers. We therefore assumed that the variations in I_{max} are not due to a change in the mechanism of cotransport, but rather reflect a difference in the number of functional cotransporters inserted in the membrane, probably due to the difference in expression levels between the different cell monolayers. We thus normalized the different sets of *I-V* relationships obtained from different cell monolayers by introducing a "standard" set of conditions as described below. For the three sets of *I-V* relations, as a function of $[HCO_3^-]_i$, collected at three different fixed $[Na^+]_i$, an additional *I-V* relation was taken at the end of each experiment under "standard zero-trans" conditions of $[HCO_3^-]_i = 57$ mM and $[Na^+]_i = 20$ mM (except for the experiment performed at the fixed $[Na^+]_i = 20$ mM, where this "standard" set of conditions was the last leg of the entire experiment). The three curves collected at each of the four $[HCO_3^-]_i$ were then corrected by normalizing with the current at zero

voltage, obtained with the "standard" conditions. The same protocol was used to normalize the three sets of *I-V* relations, as a function of $[Na^+]_i$, collected at three different fixed $[HCO_3^-]_i$. All four *I-V* relations collected under the "symmetrical" conditions were obtained from the same cell preparation (filter). Thus no normalization was performed for these *I-V* sets.

All fitting procedures were performed with the SCoPFit simulation package (SCoP Simulations, Berrien Springs, MI). The program uses the "principal axis" (praxis) algorithm to automatically search for a global minimum in the error function, by changing the initial value of each parameter by a predetermined fraction (the maximum step). A multistage approach was employed, in which the magnitude of the maximum step was progressively decreased to fine-tune the search process. The algorithm also includes occasional random jumps to avoid confinement to a local minimum. Typically, ~3000 iterations were performed, during which translocation and binding/dissociation rate constants were allowed to vary over a wide range, until a minimum in the error function (χ^2) was reached. In addition to the statistical tests, the quality of the model was also evaluated by calculating the parameter identifiability matrix and parameter sensitivity, over the tested voltage range.

Materials

Amphotericin B, bovine serum albumin, MES, HEPES, D-glucose, *N*-methyl-D-glucamine (NMDG), gluconic acid, and all salts were purchased from Sigma Chemical Co. (St. Louis, MO). Acetic acid was from Fisher Scientific. 4,4′-Dinitrostilbene-2,2′-disulfonic acid (DNDS) was obtained from Pfaltz and Bauer (Waterbury, CT). Bovine hoof collagen was a generous gift from Ethicon (Somerville, NJ).

Statistics

All experiments were repeated three times. The probability distribution for the reduced χ^2 (i.e., $P\chi^2_n$; Bevington, 1969) was used to assess the goodness of fit of model equations to experimental data, where n is the degree of freedom (i.e., number of data points − number of fitted parameters). An *F*-test analysis was used to compare different models.

RESULTS

Experimental strategy

Fig. 1 illustrates the primary transporters involved in Na^+ and HCO_3^- reabsorption in the proximal tubule (Emmett et al., 1992). The transporters associated with electrical charge movement are located in the basolateral membrane. These include the Na,K-ATPase (the Na^+ pump) and the Na-HCO_3 cotransporter. To vary the concentration of intracellular Na^+ and HCO_3^- in a controlled manner, we added 10 μM amphotericin B to the apical solution. Amphotericin B is a polyene ionophore that renders the membrane permeable to small monovalent ions (Na^+, K^+, Cl^-), but not to those with higher valences, such as Ca^{2+} (Kirk and Dawson, 1983), and stays restricted for several hours to the plasma membrane to which it was added. This property is a result of a requirement for cholesterol in the membrane, the relatively high cholesterol content of the plasma membrane, and the relatively low content of intracellular membranes (Kirk and Dawson, 1983). Permeabilization of the apical membrane with amphotericin B "removes" the electrical resistance of that membrane and reveals the basolateral electrogenic processes to external electrodes. The use of amphotericin B for the above-mentioned purposes is a common practice in studies of epithelial transport (Kirk and Dawson, 1983; Backman et al., 1992; Illek et al., 1993; Acevedo, 1994; Gross and Hopfer, 1996). In a previous study, we found that the current generated by Na,K-ATPase under short-circuit conditions interferes with measurements of currents related to Na-HCO_3 cotransporter activity (Gross and Hopfer, 1996). In the same study we also found a spontaneous increase in Cl^- conductance of the basolateral plasma membrane, which interfered with the measurement of the cotransporter conductance. Therefore, to eliminate these interference, all solutions in the present study were K^+-free (K^+ replaced by $NMDG^+$) and Cl^--free (Cl^- replaced by gluconate).

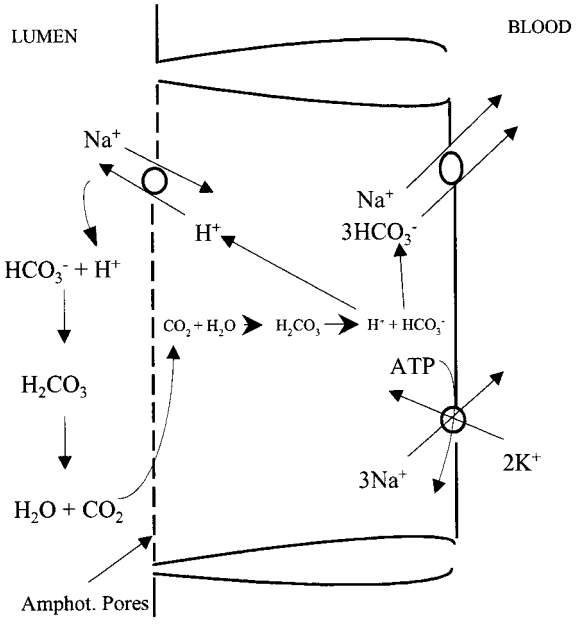

FIGURE 1 Schematic presentation of the premises on which the experiments were based. The Na-HCO_3 cotransporter transports two net negative charges. Apical application of amphotericin B functionally "removes" the apical membrane for electrical measurements.

Na-HCO_3 cotransporter activity

Sodium bicarbonate-dependent current that is sensitive to dinitrostilbene disulfide (DNDS) is taken as flux through the cotransporter. Flux through the Na-HCO_3 cotransporter can be driven by applying Na^+ and/or HCO_3^- gradients across the basolateral membrane. Fig. 2 (*upper trace*) shows the short-circuit current (I_{sc}) obtained by permeabilization of a cell monolayer preparation and subsequent experimental maneuvers. Application of a HCO_3^- gradient across the monolayer resulted in a 1.0 $\mu A/cm^2$ decrease in I_{sc}, which mainly reflects the flux of HCO_3^- from the apical to the basolateral side, and of H^+ from the basolateral to the apical side, through the tight junctions (not shown). Upon permeabilization of the apical side with 10 μM amphotericin B, a further decrease of ~2 $\mu A/cm^2$ in I_{sc} is observed. This

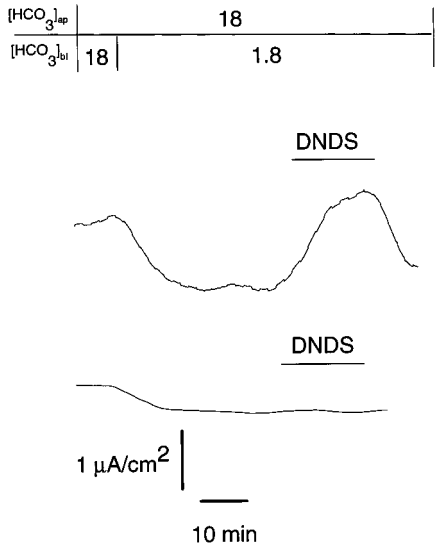

FIGURE 2 (*Upper trace*) Short-circuit current (I_{sc}) of Na-HCO_3 cotransporter driven by a HCO_3^- gradient in an apically permeabilized cell monolayer. For set-up, see Materials and Methods. Apical and basal compartments were initially perfused with a solution containing (in mM) 18.0 HCO_3^-, 20.0 Na gluconate, 100.0 NMDG, 2.5 Ca gluconate, 1.1 Mg gluconate, 50.0 HEPES, 25.0 D-glucose, and 0.1% BSA, pH 8.0. The solution was equilibrated with 1% CO_2. The cotransporter was activated by establishing a HCO_3^- gradient (apical 18.1 mM HCO_3^- to basal 1.8 mM) by lowering the pH on the basal side to 7.0. The resulting negative current returns to baseline levels upon basal application of 1 mM DNDS, as expected for flux through the cotransporter. (*Lower trace*) Imposition of a HCO_3^- gradient in the absence of Na^+ (Na^+ replaced by $NMDG^+$) caused a smaller decrease in I_{sc}, which was not affected by DNDS, and which probably reflects H^+/OH^- movements across the cell monolayer's tight junctions.

additional decrease in I_{sc} reflects the flux of Na^+ and HCO_3^- through the electrogenic basolateral Na-HCO_3 cotransporter, as judged by its sensitivity to 1 mM DNDS on the basolateral side (shown in the last segment of the experiment in Fig. 2). The inhibition by DNDS is reversible. In a separate experiment we measured a K_i of 0.11 mM for the inhibition of the cotransporter by DNDS (not shown).

In control experiments in the absence of Na^+ (Na^+ replaced with NMDG on both sides), lowering $[HCO_3^-]_{bl}$ by a similar manipulation generated a smaller decrease in I_{sc} of $\sim$0.5 $\mu A/cm^2$ (*lower trace*). This small current was not sensitive to 1 mM DNDS (*lower trace*), suggesting that it was not due to the Na-HCO_3 cotransporter. More importantly, this control experiment demonstrates the requirement for Na^+ to observe a DNDS-sensitive current under our experimental conditions (absence of K and Cl) and thus the equivalence of DNDS-sensitive current with Na-HCO_3^- cotransporter activity.

Current-voltage relationship

Kinetics of the cotransporter to Na^+ and HCO_3^- were demonstrated under two distinct experimental conditions: 1) "Zero-trans," with finite concentrations of Na^+ and HCO_3^- on the apical/intracellular side and nominally Na^+-free on the basolateral side. Furthermore, the concentration of HCO_3^- on the basolateral side was 31-fold smaller than on the apical side. 2) "Symmetrical," where the concentrations of Na^+ and HCO_3^- on one side of the basolateral membrane were equal to the concentrations of the same ions on the other side.

Zero-trans conditions

The current-voltage relationships of the cotransporter were obtained with apically permeabilized monolayers by stepping the voltage across the monolayer to different values between -160 and $+160$ mV. DNDS (1 mM) was then added to the basolateral side, and was allowed to equilibrate for 10 min before a second *I-V* relation was taken. The *I-V* curves, under zero-trans conditions, in the absence and presence of DNDS, are shown in Fig. 3 *A*. The difference between the two curves represents the DNDS-sensitive current and is shown in Fig. 3 *B*. As can be seen, the *I-V* curve is sigmoidal, with no significant positive DNDS-sensitive current at positive V_{bl}. This result is expected for zero-trans conditions, in the absence of any significant accumulation of Na^+ on the basolateral side.

$K_{0.5}^{Na}$ and I_{max}^{Na}. To study the voltage dependence of the cotransporter kinetics for Na_i^+, DNDS-sensitive *I-V* relations were collected, under zero-trans conditions, at different intracellular Na^+ concentrations and while keeping intracellular HCO_3^- concentration constant. Intracellular Na^+ concentration was varied by perfusing the apical side of an apically permeabilized cell monolayer, with solutions containing varying Na^+ concentrations. Fig. 4 *A* shows the results of such an experiment. DNDS-sensitive currents were measured at a fixed $[HCO_3^-]_i$ of 18 mM, and $[Na^+]_i$ was varied from 2.5 to 20 mM. No positive currents were observed at positive voltages, indicating effective depletion of Na^+ on the trans side.

In Fig. 4 *B*, the DNDS-sensitive currents were plotted as a function of $[Na^+]_i$ for a few potentials. As can be seen, cotransporter current increased hyperbolically with $[Na^+]_i$ and could be fitted by Eq. 1:

$$I = I_{max}^{Na}[Na^+]_i^n/((K_{0.5}^{Na})^n + [Na^+]_i^n) \quad (1)$$

where I is the DNDS-sensitive current and n is the Hill coefficient. $K_{0.5}^{Na}$ is the concentration of intracellular Na^+ required to reach half-saturation of the current I, and I_{max} is the maximum current obtained at very large $[Na^+]_i$. Cotransporter current was found to increase hyperbolically as a function of $[Na^+]_i$, with a Hill coefficient n of 1, for all potentials tested. In Fig. 5 *A* we plotted $K_{0.5}^{Na}$, as determined from Eq. 1, as a function of membrane potential at a fixed $[HCO_3^-]_i$ of 18, 30, and 57 mM. As can be seen, $K_{0.5}^{Na}$ exhibits a complex dependence on membrane potential. It decreases as the potential becomes negative, and nearly reaches a plateau in the physiological membrane potential range. In Fig. 5 *B*, we plotted $K_{0.5}^{Na}$ as a function of $[HCO_3^-]_i$

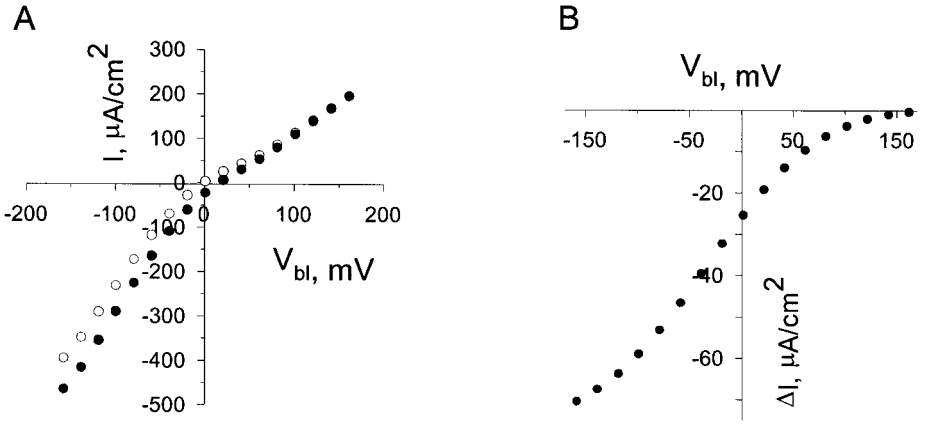

FIGURE 3 Steady-state current-voltage relationships of the outward Na-coupled HCO_3^- currents in apically permeabilized proximal tubule cells taken under "zero-trans" conditions. The current values were averaged from 10 points between 0.1 and 1.0 s at each voltage step, to eliminate possible contributions from any capacitative current transients. (*A*) Cells were perfused, on the apical side, with (in mM) 57 HCO_3^-, 20 Na gluconate, 60 NMDG, 2.5 Ca gluconate, 1.1 Mg gluconate, 100.0 HEPES, 25.0 D-glucose, and 0.1% BSA, pH 7.5. The basolateral solution contained 1.8 HCO_3^-, 80 NMDG, 2.5 Ca gluconate, 1.1 Mg gluconate, 100.0 MES, 25.0 D-glucose, and 0.1% BSA, pH 6.0. Both solutions were kept at 10% CO_2 atmosphere during the experiment, in the absence (●) and in the presence (○) of 1 mM basolateral DNDS. (*B*) Difference current-voltage relationship.

for three concentrations of HCO_3^-. As can be seen, $K_{0.5}^{Na}$ decreases monotonously with increasing $[HCO_3^-]_i$. The corresponding absolute values of I_{max}^{Na} obtained in the same experiment followed the opposite trend. I_{max}^{Na} increased as the membrane potential became more negative (Fig. 6 *A*). However, the dependence of I_{max}^{Na} on membrane potential is very different from that of $K_{0.5}^{Na}$. Fig. 6 *B* shows I_{max}^{Na} as a function of $[HCO_3^-]_i$.

$K_{0.5}^{Bic}$ and I_{max}^{Bic}. To study the voltage dependence of the cotransporter kinetics for $[HCO_3^-]_i$, DNDS-sensitive *I-V* relations were collected at different intracellular HCO_3^- concentrations while keeping the intracellular Na^+ concentration constant. $[Na^+]_{bl}$ was kept at zero levels and $[HCO_3^-]_{bl}$ was 31-fold smaller than $[HCO_3^-]_{ap}$ (zero-trans conditions). Fig. 7 *A* shows the results of such an experiment. DNDS-sensitive currents were measured at a fixed $[Na^+]_i$ of 10 mM, and $[HCO_3^-]_i$ was varied from 18 to 57 mM. In Fig. 7 *B*, DNDS-sensitive currents were plotted as a function of $[HCO_3^-]_i$ for a few potentials. As can be seen, cotransporter current increased sigmoidally with $[HCO_3^-]_i$. $K_{0.5}^{Bic}$ and I_{max}^{Bic} were determined by fitting the curves to Eq. 2:

$$I = I_{max}^{Bic}[HCO_3^-]_i^m/((K_{0.5}^{Bic})^m + [HCO_3^-]_i^m) \qquad (2)$$

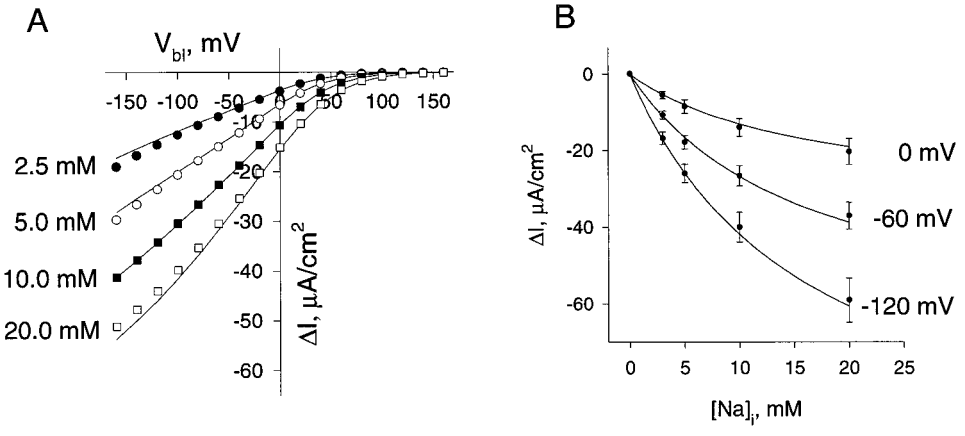

FIGURE 4 Steady-state DNDS-sensitive currents as a function of $[Na^+]_{ap}$ obtained under zero-trans conditions. (*A*) *I-V* relationships were obtained for each sodium concentration. Basolateral solutions contained (in mM) 0.6 HCO_3^-, 80 NMDG, 2.5 Ca gluconate, 1.1 Mg gluconate, 100.0 MES, 25.0 D-glucose, and 0.1% BSA, pH 6.0. The apical solution contained 18 HCO_3^-, 2.5 Ca gluconate, 1.1 Mg gluconate, 100.0 HEPES, 25.0 D-glucose, and 0.1% BSA, and varying concentrations of Na^+ (NMDG replaced by Na gluconate), pH 7.5. Solutions were kept at 3.1% CO_2 atmosphere during the experiment. The *I-V* currents were sigmoidal, approaching zero at high positive potentials and saturation at high negative potentials. The rectification at high positive potentials suggests that there is no accumulation of Na^+ and HCO_3^- on the basolateral side. Solid lines are model predictions (Eq. A13). (*B*) DNDS-sensitive currents are plotted as a function of $[Na^+]_{ap}$ at 0, −60, and −120 mV. The curves were fitted to Eq. 1 with the following parameters values: at 0 mV: $K_{0.5}^{Na} = 22 \pm 2$ mM, $I_{max}^{Na} = -32 \pm -4$ μA/cm^2; at −60 mV: $K_{0.5}^{Na} = 14 \pm 2$ mM, $I_{max}^{Na} = -53 \pm -6$ μA/cm^2; at −120 mV: $K_{0.5}^{Na} = 7.5 \pm 0.9$ mM, $I_{max}^{Na} = -60 \pm -6$ μA/cm^2.

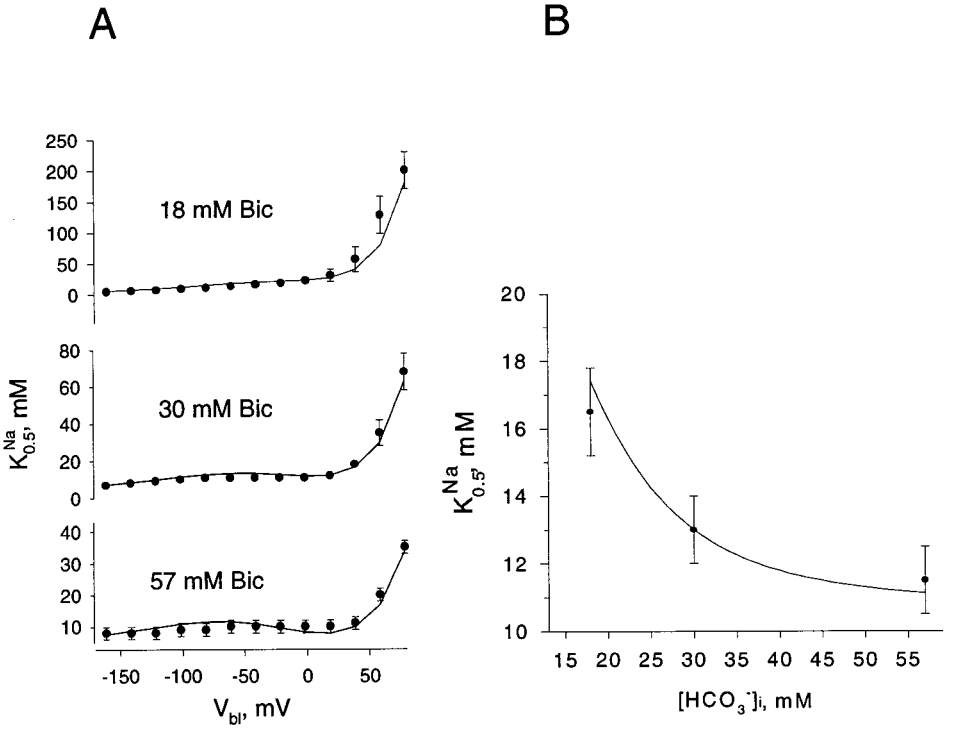

FIGURE 5 Dependence of $K_{0.5}^{Na}$, calculated from Eq. 1, on membrane potential, measured at three different HCO_3^- concentrations (*A*), and on $[HCO_3^-]_i$, measured at −60 mV (*B*), under zero-trans conditions. Solid lines represent model predictions; they were generated using Eq. A28 and the numerical values listed in Table 2.

where I is the DNDS-sensitive current and m is the Hill coefficient for bicarbonate. Cotransporter current was found to increase sigmoidally as a function of $[HCO_3^-]_i$ for all potentials tested. In Fig. 7 *C*, we plotted the Hill coefficient for bicarbonate (m_{bic}) as determined from Eq. 2 at a fixed $[Na^+]_i$ of 10 mM. As can be seen, m_{bic} equals 3, within the experimental error, over the membrane potential range of 0 to −140 mV. Thus m_{bic} does not depend on membrane potential in that range, and is in agreement with the 3 HCO_3^-:1 Na^+ stoichiometry determined previously based on thermodynamic considerations (Gross and Hopfer, 1996).

In Fig. 8 *A* we plotted $K_{0.5}^{Bic}$ as function of membrane potential at a fixed $[Na^+]_i$ of 5, 10, and 20 mM. In Fig. 8 *B*, we depicted the dependence of $K_{0.5}^{Bic}$ on $[Na^+]_i$, for three concentrations of Na_i^+. The corresponding values of I_{max}^{Bic}, obtained in the same experiment, are plotted as a function of membrane potential in Fig. 9 *A*, and as a function of $[Na^+]_i$ in Fig. 9 *B*.

Symmetrical conditions

The *I-V* relationship for the cotransporter at different Na^+ concentrations revealed an increase in conductance at increasing Na^+ concentrations (not shown). When measuring the *I-V* relationship at different HCO_3^- concentrations, we observed an increase in current at concentrations up to 40 mM. Interestingly, increasing the HCO_3^- concentration above 40 mM caused a decrease in the current (not shown). This effect probably results from trans-inhibition by baso-

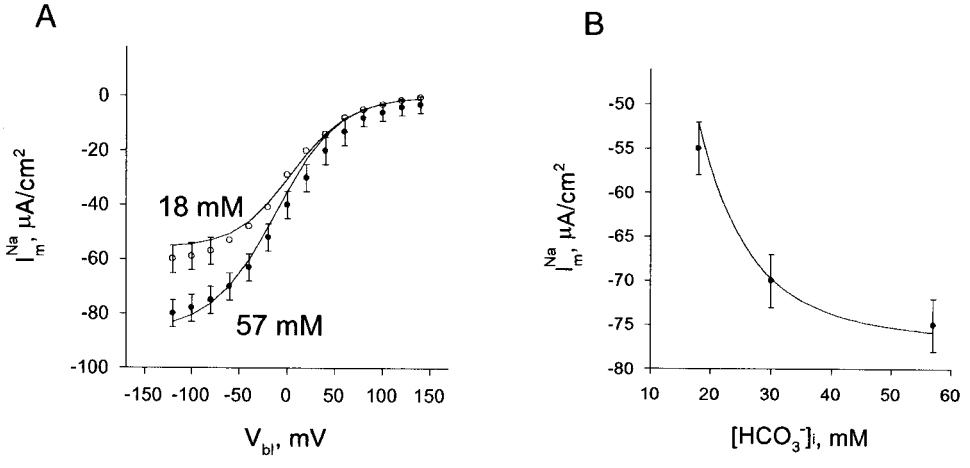

FIGURE 6 Dependence of I_{max}^{Na}, calculated from Eq. 1, on membrane potential, measured at 18 and 57 mM HCO_3^- (*A*), and on $[HCO_3^-]_i$, measured at −60 mV (*B*), under zero-trans conditions. Solid lines represent model predictions; they were generated using Eq. A27 and the numerical values listed in Table 2.

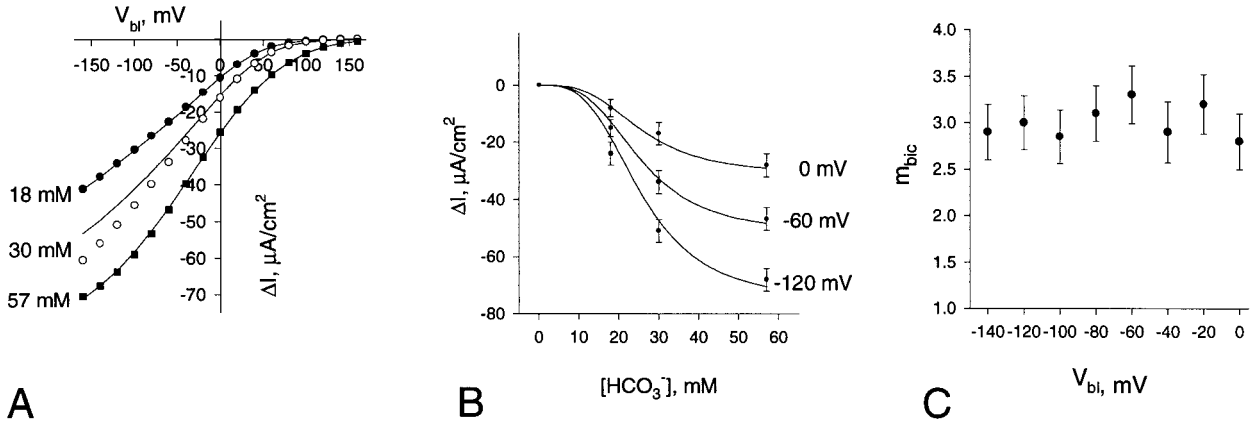

FIGURE 7 Steady-state DNDS-sensitive currents as a function of $[HCO_3^-]_{ap}$ obtained under zero-trans conditions. (*A*) *I-V* relationships were obtained with a fixed $[Na^+]_{ap}$ of 10 mM, and 18 mM (●), 30 mM (○), and 57 mM HCO_3^- (■). Basolateral solutions contained (in mM) 80 NMDG, 2.5 Ca gluconate, 1.1 Mg gluconate, 100.0 MES, 25.0 D-glucose, and 0.1% BSA, pH 6.0. The apical solution contained 2.5 Ca gluconate, 1.1 Mg gluconate, 100.0 HEPES, 25.0 D-glucose, and 0.1% BSA, and varying concentrations of HCO_3^-, pH 7.5. $[HCO_3^-]_{ap}$ was varied from 18 mM to 57 mM by increasing pCO_2 and allowing the solutions to equilibrate for 1 h before the next *I-V* relation was taken ($[HCO_3^-]$ was calculated from the Henderson-Hasselbalch relation as explained in Materials and Methods). Solid lines are model predictions (Eq. A13). (*B*) DNDS-sensitive currents are plotted as a function of $[Na^+]_{ap}$ at 0, −60, and −120 mV. The curves were fitted to Eq. 2 with the following parameters: at 0 mV: $K_{0.5}^{Bic} = 21 \pm 2$ mM, $I_{max}^{Bic} = -27 \pm -2$ μA/cm²; at −60 mV: $K_{0.5}^{Bic} = 19 \pm 2$ mM, $I_{max}^{Bic} = -56 \pm -5$ μA/cm²; at −120 mV: $K_{0.5}^{Bic} = 17 \pm 2$ mM, $I_{max}^{Bic} = -65 \pm -5$ μA/cm². (*C*) Voltage dependence of the Hill coefficient, *m*, for bicarbonate as calculated from fitting the data described in Fig. 7 *B* to Eq. 2. *m* was voltage independent, with values ranging from a minimum of 2.9 ± 0.3 at −100 mV to a maximum of 3.3 ± 0.3 at −60 mV.

lateral HCO_3^-. Trans-inhibition was reported for various cotransporters (Stein, 1990, p. 199), and can be explained on the basis of solute on the trans side inducing the formation of the nonproductive carrier form on that side of the membrane, thereby "removing" carrier available for supporting transport.

Transport model

Assumptions and rationale

Four topological alternative schemes of a six-state ordered binding model were analyzed for their ability to fit the *I-V* data sets: 1) Na_i^+ first on–last off (F-L); 2) Na_i^+ first on–first off (F-F); 3) Na_i^+ last on–first off (L-F); and 4) Na_i^+ last on–last off (L-L). Fig. 10 is a schematic presentation of the four different schemes. The model is said to be ordered, because one substrate has to bind to the carrier before the other substrate can bind. In all four schemes, the carrier possesses one binding site for Na^+ and three binding sites for HCO_3^-. Bicarbonate is assumed to bind in sequential steps that were lumped together. The binding of three bicarbonate ions to the cotransporter is therefore described and treated analogously to a bimolecular rate so that familiar model nomenclature could be employed. It should be

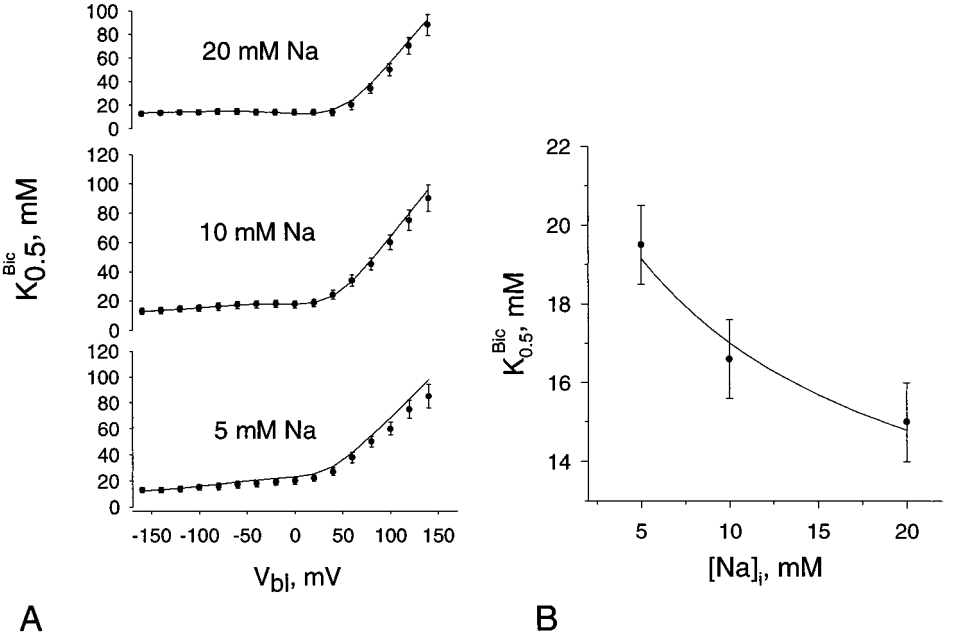

FIGURE 8 Dependence of $K_{0.5}^{Bic}$, calculated from Eq. 2, on membrane potential, measured at 5, 10, and 20 mM Na^+ (*A*), and on $[Na^+]_i$, measured at −60 mV (*B*), under zero-trans conditions. Solid lines represent model predictions; they were generated using Eq. A31 and the numerical values listed in Table 2.

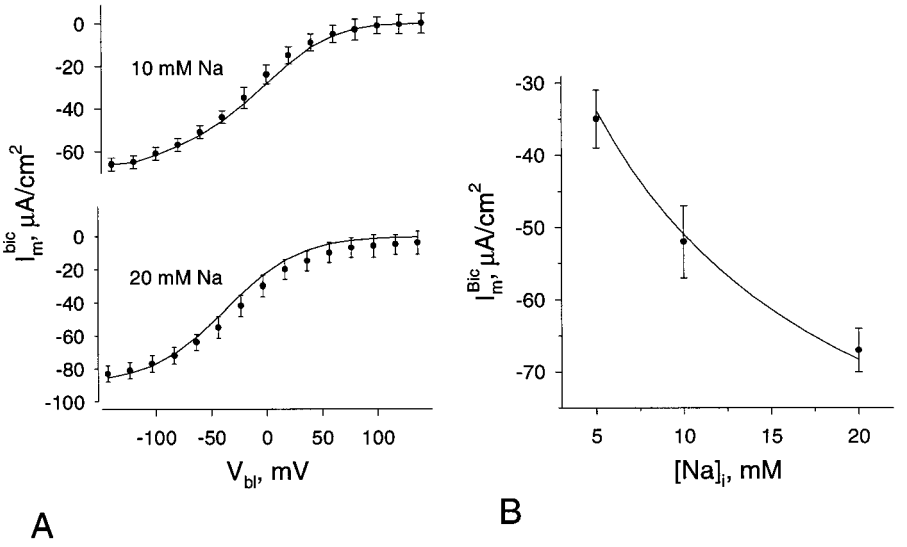

FIGURE 9 Dependence of I_{max}^{Bic}, calculated from Eq. 2, on membrane potential, measured at 10 and 20 mM Na^+ (*A*), and on $[Na^+]_i$, measured at −60 mV (*B*), under zero-trans conditions. Solid lines represent model predictions; they were generated using Eq. A30 and the numerical values listed in Table 2.

mentioned that while most studies on the proximal tubular Na-HCO_3 cotransporter report a HCO_3^-:Na^+ stoichiometry of 3:1, one group reported a stoichiometry of 1 HCO_3^-:1 $CO_3^=$:1 Na^+ (Soleimani and Aronson, 1989). We did not treat this case in this study. The model consists of one transport loop linking six discrete states of the carrier. Only the empty (C) and fully loaded (NaC3HCO_3) forms of the carrier are assumed to be able to translocate across the membrane. This assumption is consistent with the observations that no CO_2-dependent DNDS-sensitive current could be observed in the absence of Na^+ (Fig. 2), and that no Na^+-dependent DNDS-sensitive current could be observed in the absence of CO_2 (not shown).

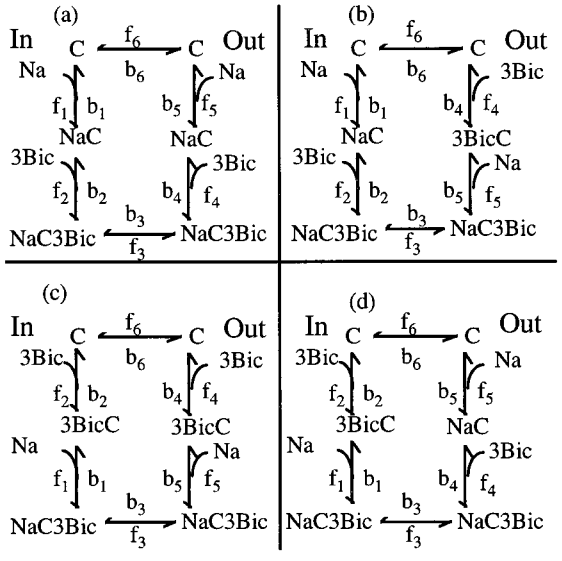

FIGURE 10 Different binding schemes of a six-state ordered-binding transport model of the Na-HCO_3 cotransporter. (*a*) Na_i^+ first on–last off. (*b*) Na_i^+ first on–first off. (*c*) Na_i^+ last on–first off. (*d*) Na_i^+ last on–last off. The rate constants for the forward (f_i) and backward (b_i) reactions are modulated by voltage and/or ligand concentration as described by Eqs. 3–14. The binding of three HCO_3^- anions to the carrier is described as a single, lumped step (see text).

In addition to the two transmembrane steps, the model contains individual steps for binding and release of Na^+ and HCO_3^- at each side of the membrane. No constrains with respect to the limiting step in the catalytic cycle were imposed in our model. Furthermore, each rate constant was allowed to become voltage dependent. Membrane surface charges and unstirred layer effects at the membrane boundaries were assumed to be negligible (i.e., substrate concentrations were considered to be uniformly distributed between the membrane surface and the bulk aqueous phase).

An ordered model is a submodel of a more general random binding model, in which the rate of one of the two branches (that describes substrate binding) is much slower than that of the other branch and thus can be ignored. Because of their greater topological complexity, which results in an inherent ability to describe a wide variety of kinetic data, non-rapid-equilibrium random-binding models are used to interpret bi- or multiphasic kinetic data that do not obey simple, monophasic Michaelis-Menten kinetics. Because the presence of Michaelis-Menten kinetics is an indication of an ordered binding mechanism (Segel, 1975), and because the kinetics of Na^+ and HCO_3^- transport in this study could be reasonably well described by monophasic Michaelian kinetics, we found no justification for extension of the analysis to systems involving yet more carrier states.

Ping-pong mechanisms were considered, but can be excluded as explained below. Ping-pong mechanisms are those for which transport intermediates with both sodium and bicarbonate bound do not exist. For this class of mechanisms, the half-saturation constant ($K_{0.5}$) and the maximum current (I_{max}) for bicarbonate-dependent fluxes vary by the same factor as that by which the sodium concentration is changed (Stein, 1984). Because the two solutes bind alternately at opposite sides of the membrane to different carrier conformational states, the ratio of I_{max}^{Bic} to $K_{0.5}^{Bic}$, in a ping-

pong model, should remain constant as $[Na^+]_i$ is varied. Because $I^{Bic}_{max}/K^{Bic}_{0.5}$ strongly depends on $[Na^+]_i$, as Table 1 shows, ping-pong models can be discarded.

Formal model description

Effect of membrane potential on transport rate constants

The effect of membrane potential on ion binding and dissociation reaction steps and on the translocation of the loaded carrier is conveniently described by the Eyring theory of reaction rates (Eyring et al., 1949; Woodbury, 1971). The binding of sodium and bicarbonate to the carrier protein and the translocation of these ions by the carrier across the membrane may be described as a series of activated processes in which Na^+ and HCO_3^- hop across a series of symmetrical Eyring energy barriers. The energy barrier, for each step in the cycle, is modulated by the fraction of the membrane electric field sensed by that voltage-dependent step. The modulation factor is given by $e^{-\zeta x u/2}$, where ζ is the valence of the carrier species corresponding to that step, x is the corresponding fraction of the membrane potential sensed by that step, u is the reduced, dimensionless, membrane potential, $u = FV/RT$, where V is the membrane potential, and F, R and T have their usual meanings. The factor 1/2 in the exponent indicates symmetry in the Eyring barrier (in a more general form of the equation, this factor could be replaced with a separate parameter to indicate the position of the barrier peak in the membrane). The general form of the apparent rate constants for model *a* in Fig. 10 are given below:

$$f_1 = f_1^o[Na]_i^n \exp(n\alpha' u/2)$$

binding of intracellular Na^+ to the carrier (3)

$$b_1 = b_1^o \exp(-n\alpha' u/2)$$

dissociation of intracellular Na^+ from the carrier (4)

$$f_2 = f_2^o[HCO_3]_i^m \exp(-m\beta' u/2)$$

binding of intracellular HCO_3^- to the carrier (5)

$$b_2 = b_2^o \exp(m\beta' u/2)$$

dissociation of intracellular HCO_3^- from the carrier (6)

TABLE 1 Sodium dependence of bicarbonate kinetics parameters

$[Na^+]_i$ (mM)	I^{Bic}_{max} (μA/cm^2) (mean ± SD)	$K^{Bic}_{0.5}$ (mM) (mean ± SD)	$I^{Bic}_{max}/K^{Bic}_{0.5}$ (μA/cm^2 · mM) (mean ± SD)
10	−50 ± 3.1	19 ± 1.2	2.6 ± 0.32
20	−70 ± 6.2	15 ± 1.1	4.7 ± 0.76

$$f_3 = f_3^o \exp((z\delta_z + n\delta_n - m\delta_m)u/2)$$

translocation of the loaded carrier (inside → outside) (7)

$$b_3 = b_3^o \exp(-(z\delta_z + n\delta_n - m\delta_m)u/2)$$

translocation of the loaded carrier (outside → inside) (8)

$$f_4 = f_4^o \exp(-m\beta'' u/2)$$

dissociation of extracellular HCO_3^- from the carrier (9)

$$b_4 = b_4^o[HCO_3]_o^m \exp(m\beta'' u/2)$$

binding of extracellular HCO_3^- to the carrier (10)

$$f_5 = f_5^o \exp(n\alpha'' u/2)$$

dissociation of extracellular Na^+ from the carrier (11)

$$b_5 = b_5^o[Na]_o^n \exp(-n\alpha'' u/2)$$

binding of extracellular Na^+ to the carrier (12)

$$f_6 = f_6^o \exp(-z\delta_z u/2)$$

translocation of the unloaded carrier (outside → inside) (13)

$$b_6 = b_6^o \exp(z\delta_z u/2)$$

translocation of the unloaded carrier (inside → outside) (14)

where z is the valence of the empty carrier, n and m are the number of Na^+ and HCO_3^- ions being transported, and δ_n and δ_m represent the fractions of the electric field through which Na^+ and HCO_3^- ions, respectively, move with transport across the membrane. δ_z is the corresponding parameter that describes the fraction of the electric field sensed by the charge on the unloaded carrier (z) as it traverses the membrane. α' and α'' represent the fraction of the electric field sensed by the binding steps of cytoplasmic and extracellular Na^+, respectively, and $\alpha' + \alpha'' + \delta_n = 1$ (see also Jauch and Läuger, 1986). β' and β'' represent the corresponding parameters for bicarbonate, with $\beta' + \beta'' + \delta_m = 1$. It should be noted that no constraint or limits can be written to describe the translocation of the charge z across the membrane. This is because, unlike the Na^+ and HCO_3^- ions, the charge z does not necessarily traverse the entire distance of membrane thickness, upon translocation of the substrates across the membrane. The product $z\delta_z$ can thus assume any value. Furthermore, z and δ_z cannot be determined separately. The product $z\delta_z$ will thus be referred to as the "effective charge" of the unloaded carrier.

Current equation

The general equation for the steady-state carrier current is given by the sum of all possible translocation steps:

$$I = -F\{z\delta_z(b_6C_1 - f_6C_6) + (z\delta_z + n - m)(f_3C_3 - b_3C_4)\} \quad (15)$$

where C_x is the concentration of the corresponding carrier state (see Fig. 10 *a*). Two methods were employed to solve for C_x in terms of the rate constants, as described below. The two methods gave identical results.

Method I: King-Altman diagrams

This is a diagrammatic method that can be used to solve, analytically, for the steady-state concentration of individual carrier state concentration (C_x) in terms of the transport cycle rate constants and the total concentration of the carrier (C_T). The concentration of C_x is given by the sum of six King-Altman terms, each of which is the product of five different rate constants (see Appendix).

Method II: Integration of the rate equations

The rate at which each of the carrier species concentration changes is given by the difference of the forward and reverse reactions that lead to and from that state. The set of differential equations that describe the change in concentration of each state can be solved, numerically, by numerical solver routines for any desired time interval. The steady-state solution of the set was obtained using the "kinetic" solver of the SCoP simulations package, by assigning a large value (10^9 s) to the time step. The set of differential equations that describe the rate of change in the concentration of a carrier state, for the F-L scheme, is given below:

$$dC_1/dt = (b_1C_2 + f_6C_6) - (f_1 + b_6)C_1 \quad (16)$$

$$dC_2/dt = (f_1C_1 + b_2C_3) - (b_1 + f_2)C_2 \quad (17)$$

$$dC_3/dt = (f_2C_2 + b_3C_4) - (b_2 + f_3)C_3 \quad (18)$$

$$dC_4/dt = (f_3C_3 + b_4C_5) - (b_3 + f_4)C_4 \quad (19)$$

$$dC_5/dt = (f_4C_4 + b_5C_6) - (b_4 + f_5)C_5 \quad (20)$$

$$dC_6/dt = (f_5C_5 + b_6C_1) - (b_5 + f_6)C_6 \quad (21)$$

Simulation and fitting procedures

Numerical values of rate constants and electrical coefficients were obtained by simultaneously fitting the *I-V* relationships collected under "zero-trans" and "symmetrical" conditions to Eq. 15. Eleven of the 12 rate constants were assigned an initial guess value; the 12th constant (b_6) was calculated from the other 11 constants by using the mass action (microscopic reversibility) law:

$$b_6^o = f_1^o f_2^o f_3^o f_4^o f_5^o f_6^o / b_1^o b_2^o b_3^o b_4^o b_5^o \quad (22)$$

The electrical coefficients α', α'', β', and β'' were allowed to vary between 0 and 1 during the iterative process. n and m were assigned the values 1 and 3, respectively, based on the 1 Na^+:3 HCO_3^- stoichiometry determined previously (Gross and Hopfer, 1996), and were not allowed to vary during iterations. C_T was assigned a fixed value of 2 pmol/cm^2 and was not allowed to vary during iterations. This corresponds to a surface density of ~10,000 molecules/μm^2. For comparison, the surface density of the anion transporter (band 3) of erythrocytes was estimated to be 8000 carriers/μm^2 (Stein, 1990, p. 156). Carrier translocation rate constants were assigned initial values of 1 s^{-1}, and binding and dissociation rate constants were assigned initial values of 10,000 s^{-1}, s^{-1} M^{-1}, or s^{-1} M^{-3}. Simulation were performed until one set of rate constants was found that simultaneously fit all of the *I-V* sets, rather than aiming at multiple solutions that could account for only one *I-V* set. The numerical values of the rate constants obtained by fitting the *I-V* curves to the F-L model (i.e., Na^+ first on and last off) are listed in Table 2. All four ordered binding schemes gave similar numerical values. The numerical values, listed in Table 2, were then used to fit the data sets of I_{max} and $K_{0.5}$, for a given substrate as a function of the concentration of the cosubstrate and as a function of membrane potential. This can be done by rearranging the current equation in a phenomenological (Michaelis-Menten) form (see the Appendix). It should be noted that because the model was solved numerically, rather then analytically, the set of numerical values listed in Table 2 might not represent a unique solution of the model, and other solutions may exist.

TABLE 2 Fitted parameters for the ordered binding model F-L

Parameter	Initial value	Final value	Limits
$z\delta_z$	1.0	2.00	$-5 \le z\delta_z \le 5$
α'	0.5	0.00	$0 \le \alpha' \le 1$
α''	0.5	0.00	$0 \le \alpha'' \le 1$
β'	0.5	0.12	$0 \le \beta' \le 1$
β''	0.5	0.00	$0 \le \beta'' \le 1$
f_1^o	10^4 M^{-1} s^{-1}	557.9 M^{-1} s^{-1}	$0 \le f_1^o \le 10^9$
b_1^o	10^4 s^{-1}	41.7 s^{-1}	$0 \le b_1^o \le 10^9$
f_2^o	10^4 M^{-3} s^{-1}	$1.1 \cdot 10^6$ M^{-3} s^{-1}	$0 \le f_2^o \le 10^9$
b_2^o	10^4 s^{-1}	899.6 s^{-1}	$0 \le b_2^o \le 10^9$
f_3^o	1.0 s^{-1}	596.9 s^{-1}	$0 \le f_3^o \le 10^9$
b_3^o	1.0 s^{-1}	575.6 s^{-1}	$0 \le b_3^o \le 10^9$
f_4^o	10^4 s^{-1}	125.0 s^{-1}	$0 \le f_4^o \le 10^9$
b_4^o	10^4 M^{-3} s^{-1}	216471 M^{-3} s^{-1}	$0 \le b_4^o \le 10^9$
f_5^o	10^4 s^{-1}	0.3 s^{-1}	$0 \le f_5^o \le 10^9$
b_5^o	10^4 M^{-1} s^{-1}	38.6 M^{-1} s^{-1}	$0 \le b_5^o \le 10^9$
f_6^o	1.0 s^{-1}	0.7 s^{-1}	$0 \le f_6^o \le 10^9$
b_6^o		0.06 s^{-1}	$0 \le b_6^o \le 10^9$
C_T	2 pmol/cm^2		
n	1		
m	3		

All four ordered-binding schemes gave similar parameter values ($P\chi_n^2 > 0.95$). All parameters were identifiable over the range of voltages tested.

Submodels

The model presented above was obtained by making the least number of simplifying assumptions that are practical. Thus we will refer to it as the general model. In the discussion that follows we will consider some simple cases (or submodels) of the general model. The validity of the assumptions used to derive the submodels will be assessed by comparing the error function (χ^2_n) for each case with that of the general model.

Rapid equilibrium models

If intracellular Na^+ or HCO_3^- binding to the cotransporter is rapid compared to the translocation steps, then the binding reactions of these ions to the cotransporter are said to be in "rapid equilibrium." Because it reduces the complexity of the algebra required to model cotransport activity, rapid-equilibrium assumptions of substrate binding have been the most enduring working hypotheses in the analysis of other Na^+-dependent cotransport systems (Goldner et al., 1969; Restrepo and Kimmich, 1985; Jauch and Läuger, 1986). The rapid equilibrium assumption has been questioned by many in the field (Sanders et al., 1984; Sanders, 1986; Schultz, 1986; Weirzbicki et al., 1990). As discussed above, rapid binding/dissociation of substrate was not assumed in deriving our general model. Thus, all of the 11 rate constants were allowed to vary within the same range (i.e., $0–10^9$) during the fitting. To evaluate the effect on our model of assuming that Na^+ and HCO_3^- binding/dissociation is fast compared to the membrane translocation steps, the lower limit of the range over which the rate constants for substrate binding/dissociation could vary was set higher (10^4 to 10^9) than the corresponding range for the translocation rate constants (0 to 10^3). The latter range encompasses the translocation rate constants predicted by the general model (see Table 2). The experimental data were then refitted to the model with the new range limits, and the error (χ^2_n) was calculated. These manipulations test the effect of "forcing" rapid binding/dissociation rates, but, in effect, without restricting the translocation rates.

If the rapid binding/dissociation assumption is valid, then this manipulation should not affect, or even improve, the goodness of fit of the data to the submodel and, hence, the value of the error function. Table 3 compares χ^2_n obtained for assuming rapid binding/dissociation for Na^+, HCO_3^-, or Na^+ and HCO_3^-. As Table 3 suggests, even for "partial rapid equilibrium" submodels (i.e., when only one of the substrates is assumed to rapidly bind/dissociate), the goodness of fit is compromised compared to that obtained with the general model. Thus we conclude that the rapid binding/dissociation assumption, for Na^+, HCO_3^-, or both, is not justified.

TABLE 3 Effect of forcing rapid binding/dissociation of Na^+ and HCO_3^- on the goodness-of-fit (χ^2_n)

	Statistical parameter	
Binding/dissociation of	χ^2_n	$P(\chi^2_n)$
Unrestricted	0.81	>0.95
Na^+ and HCO_3^-	1.08	<0.2
Na^+	0.92	<0.7
HCO_3^-	1.02	<0.5

Rapid binding/dissociation assumptions were forced by setting the limits of the translocation rate constants (f_3, b_3 and f_6, b_6) at $0–10^3$. This range encompasses the numerical values of these constants obtained with the general model (see Table 2). The range of Na^+ or HCO_3^- binding and dissociation rate constants (f_1, b_1 and f_5, b_5 or f_2, b_2 and f_4, b_4), respectively, was set to 10^4 to 10^9. The initial guess values for these parameters were the same as in Table 2.

Voltage-independent binding of HCO_3^-

Our general model predicts that all binding steps, except that of intracellular HCO_3^- to the cotransporter, are voltage-independent. The binding of intracellular HCO_3^- "senses" about 12% of the membrane's electric field (i.e., $\beta' = 0.12$). In this submodel we test the effect of assuming that all binding steps, including that of intracellular HCO_3^-, are voltage independent. This restriction is equivalent to the assumption that the translocation of the bound ions, by the cotransporter, through the membrane "senses" 100% of the transmembrane electric field. This was done by setting α', α'', β', $\beta'' = 0$ and refitting the data to the submodel. These settings were held fixed during the fitting process. χ^2_n obtained for this model was 1.34 compared to 0.81 for the general model. Therefore the assumption that all binding steps are voltage independent is not justified.

Other ordered-binding models

In deriving the general model we assumed that the binding of 3 HCO_3^- on either side of the membrane can be lumped into one step, which can occur either after (F-L) or before (L-F) the binding of Na^+. To check whether the lumping assumption was justified, we fitted the *I-V* data to the following ordered-binding model: $1HCO_{3i}^-$, 1 Na_i^+, $2HCO_{3i}^- \leftrightarrow 2HCO_{3o}^-$, 1 Na_o^+, $1HCO_{3i}^-$ (i.e., HCO_3^- binds first, followed by Na^+, followed by 2 HCO_3^-). The numerical values of the rate constants, electrical coefficients, and error obtained by this model were comparable to those obtained by the original "lumped" model. Thus, although our data are consistent with a "lumped" model, other ordered binding models, i.e., in which Na^+ binds after the first HCO_3^-, cannot be ruled out.

DISCUSSION

The proximal tubular Na-HCO_3 cotransporter is electrogenic. Because both substrates are being transported against their respective concentration gradients across the basolateral membrane, the only driving force for the transport process is the inside-negative membrane potential. Thus any change in basolateral membrane potential would affect the flux through the cotransporter. The relationship between

changes in the flux through the cotransporter and changes in the membrane potential is determined by the voltage sensitivity of the different steps in the transport cycle and the charge on the cotransporter. In this study we present a model that describes the dependence of the flux on membrane potential in terms of the voltage sensitivity of individual steps in the transport cycle. The model can account for the dependence of the flux on membrane potential and on substrate concentration. In this section we will discuss the main postulates of the model.

Rate constants

The present model predicts that the translocation of the loaded carrier through the membrane, at zero voltage, is ~10,000-fold faster than that of the unloaded form. A similar relationship, whereby the translocation of the loaded carrier is faster than that of the empty form, was also reported for the anion exchanger (Band 3) of erythrocytes (Stein, 1990, pp. 160–161). In the latter case, the large difference in translocation rates between the loaded and unloaded forms of the carrier ensures that the transporter operates in an exchange mode, whereby a HCO_3^- anion is exchanged for a Cl^- anion. The significance of the large difference in the translocation rates for the Na-HCO_3 cotransporter is, at the present, unclear. Another cotransport system in which the loaded form of the carrier was reported to translocate faster than the unloaded form is the Na-glucose cotransporter, although in this case the ratio of translocation rates was smaller, i.e., on the order of ~100-fold (Hopfer and Groseclose, 1980; Kessler and Semenza, 1983; Kimmich and Randles, 1984; Stevens et al., 1984). The large ratio of the rate constants for translocation between loaded and unloaded forms of the carrier is not necessarily an intrinsic property of the transporter protein. It could result from the difference in net charge movement associated with translocation of the two forms, in conjunction with static surface or dipole potentials (Bedlack et al., 1994; Gross et al., 1994). For example, even if the loaded and unloaded forms had the same transition state for the translocation across the membrane barrier, activation energies and hence rate constants for translocation would be different, depending on the electrical potential of the transition relative to the ground states. Thus a ratio of 10,000 can be accounted for by the relatively small electrostatic potential difference of +120 mV between the transition and ground states, given the difference of $\Delta Z = +2$ electrical charges between unloaded and loaded carrier forms.

I-V curves and phenomenological constants

The model predicts the dependence of the phenomenological constants $K_{0.5}^{Na}$ on membrane potential and $[HCO_3^-]_i$ (Fig. 5, *A* and *B*). Fig. 5 *A* exhibits a triphasic dependence of $K_{0.5}^{Na}$ on membrane potential, with a slight increase between −150 and −50 mV, then a decrease between −50 and +10 mV, and then a sharp increase at large positive potentials. Although the physical origin of such a triphasic voltage profile is currently unclear, computer simulations indicate that it becomes more pronounced at high concentrations of HCO_3^- on the trans side and completely disappear at zero trans concentration. The dependence of $K_{0.5}^{Na}$ (Fig. 5 *B*) and I_{max}^{Na} (Fig. 6 *B*) on $[HCO_3^-]_i$ provide a mechanism by which changes in the latter, around the physiological level, may regulate the activity of the cotransporter. Similarly, the steep dependence of $K_{0.5}^{Bic}$ (Fig. 8 *B*) and of I_{max}^{Bic} (Fig. 9 *B*) on $[Na^+]_i$ suggests that changes in intracellular Na^+ may play a role in the regulation of the activity of the cotransporter by affecting these kinetic parameters. An interesting observation is that although the rate constants of intra- and extracellular sodium binding and dissociation do not depend on membrane potential (α', $\alpha'' = 0$; Table 2), $K_{0.5}^{Na}$ and I_{max}^{Na} do exhibit voltage sensitivity (Figs. 5 *A* and 6 *A*, respectively). This voltage sensitivity is the result of voltage sensitivity of intracellular bicarbonate binding as reflected by the voltage sensitivity of f_2 ($\beta' = 0.12$).

In Fig. 11, we plotted the dependence of the cotransporter current on the concentration of its two ligands under symmetrical conditions, according to Eq. A13. Because $[HCO_3^-]$ and $[Na^+]$ represent two independent variables, the resulting three-dimensional plot describes an "activity surface." As can be seen, the current surface exhibits a maximum. The decrease in cotransporter current at high HCO_3^- concentration is due to a trans-inhibition effect of this substrate (see also Stein, 1990, p. 199, for a general discussion on trans-inhibition in other cotransport systems). Trans-inhibition effects were also reported for the Na-glucose cotransporter, where intracellular Na^+ or sugar was found to exert a pronounced inhibitory effect on the unidirectional influx of sugar via the phlorizin-sensitive cotransport system (Kessler and Semenza, 1983; Dorando and Crane, 1984; Schultz and Curran, 1970; Semenza, 1971). One problem limiting easy interpretation of the magnitude of trans-inhibitory effects in those studies is the fact that the experimental procedures that were used to elevate cellular sodium also depolarized the cell membrane potential. Therefore, it is difficult to know which part of the observed trans-inhibitory effect is due to an increase in cell sodium and which part is due to concomitant depolarization of the membrane potential. Indeed, when the potential was experimentally maintained with the aid of imposed diffusion potentials after loading of the cells with sodium, the potency of intracellular sodium as an inhibitor was greatly reduced (Kimmich and Randles, 1988). This problem does not exist in our experimental system, as the membrane potential is clamped to a fixed value with external electrodes, and thus does not depend on the concentrations of the solutes.

The proximal tubule plays an important role in the reabsorption of sodium in the kidney. Although the main exit pathway of Na^+ across the basolateral membrane is through the Na,K-ATPase, this pathway is energetically "expensive," as it requires the hydrolysis of ATP. By coupling the

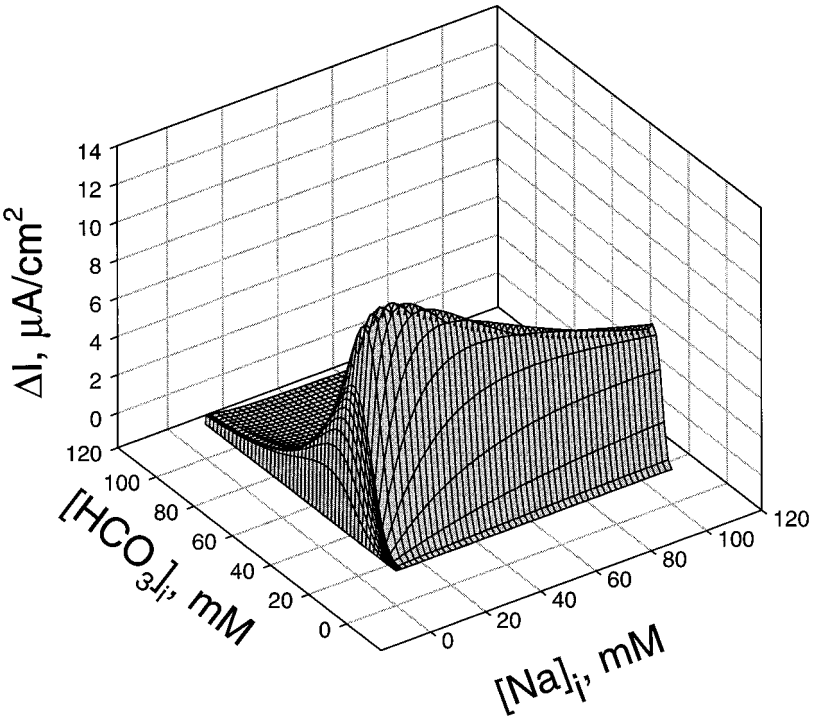

FIGURE 11 Three-dimensional surface plot of cotransporter current as a function of $[Na^+]_i$ and $[HCO_3^-]_i$ under symmetrical conditions. The plot was generated using Eq. A13 and the numerical values shown in Table 2, at a membrane potential of −60 mV.

transport of Na^+ to that of HCO_3^-, the cell utilizes the inside-negative membrane potential to transport Na^+ out of the cell, and can thus save cellular ATP.

APPENDIX

Ordered binding model

Steady-state concentrations of each carrier form were solved using the diagrammatic method of King and Altman (1956). Fig. 12 shows the six different King-Altman patterns for the F-L ordered binding model. The concentration of a given carrier form [Cx] is then given by

$$[C_x] = \frac{\sum_{j=1}^{6} T_x^j}{\sum_{i=1}^{6}\sum_{j=1}^{6} T_i^j} \cdot C_T \tag{A1}$$

C_T is the macroscopic surface density of cotransporter in units of mol/cm^2. C_T must be measured independently, e.g., by using electrical relaxation techniques (see, for example, Läuger, 1972). No attempt was made to measure C_T in this work. T_i^j is an individual King-Altman term, where i is the carrier state and j is one of the King-Altman patterns. Each term is the product of five apparent rate constants determined by multiplying the rate constants around the paths outlined in Fig. 12. The six different states of the carrier are given below:

$$\Sigma C_1 = b_1b_2b_3b_4f_6 + b_1b_2b_3f_5f_6 + b_1b_2f_4f_5f_6 + b_1f_3f_4f_5f_6 + f_2f_3f_4f_5f_6 + b_1b_2b_3b_4b_5 \tag{A2}$$

$$\Sigma C_2 = f_1b_1b_3b_4f_6 + f_1b_2b_3f_5f_6 + f_1b_2f_4f_5f_6 + f_1f_3f_4f_5f_6 + f_1b_2b_3b_4b_5 + b_6b_2b_3b_4b_5 \tag{A3}$$

$$\Sigma C_3 = f_1f_2b_3b_4f_6 + f_1f_2b_3f_5f_6 + f_1f_2f_4f_5f_6 + b_6b_1b_3b_4b_5 + f_1f_2b_3b_4b_5 + b_6f_2b_3b_4b_5 \tag{A4}$$

$$\Sigma C_4 = f_1f_2f_3f_4f_6 + f_1f_2f_3f_5f_6 + b_6b_1b_2b_4b_5 + b_6b_1f_3b_4b_5 + f_1f_2f_3b_4b_5 + b_6f_2f_3b_4b_5 \tag{A5}$$

$$\Sigma C_5 = f_1f_2f_3f_4f_6 + b_6b_1b_2b_3b_5 + b_6b_1b_2f_4b_5 + b_6b_1f_3f_4f_5 + f_1f_2f_3f_4b_5 + b_6f_2f_3f_4b_5 \tag{A6}$$

$$\Sigma C_6 = b_6b_1b_2b_3b_4 + b_6b_1b_2b_3f_5 + b_6b_1b_2f_4f_5 + b_6b_1f_3f_4f_5 + f_1f_2f_3f_4f_5 + b_6f_2f_3f_4f_5 \tag{A7}$$

Conservation of mass requires that

$$C = \Sigma C_1 + \Sigma C_2 + \Sigma C_3 + \Sigma C_4 + \Sigma C_5 + \Sigma C_6 \tag{A8}$$

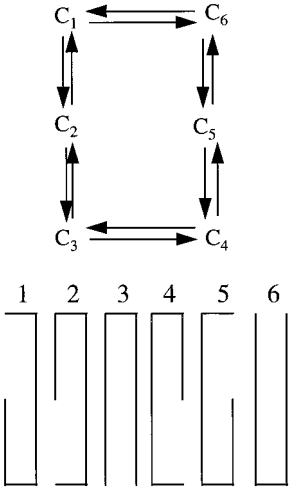

FIGURE 12 King-Altman patterns for carrier states of the F-L scheme. Each carrier state is identified by a number ranging from 1 to 6.

Current equation

The steady-state cotransporter current equation for the F-L ordered binding model is determined by the sum of the two membrane translocation steps:

$$I = -F\{z\delta_z(b_6C_1 - f_6C_6) + (z\delta_z + n - m)(f_3C_3 - b_3C_4)\} \tag{A9}$$

where C_1, C_6, C_3, and C_4 are given by

$$C_1 = (\Sigma C_1/C)C_T; \qquad C_6 = (\Sigma C_6/C)C_T \tag{A10}$$

$$C_3 = (\Sigma C_3/C)C_T; \qquad C_4 = (\Sigma C_4/C)C_T \tag{A11}$$

Using thermodynamic considerations, we previously determined the cotransport stoichiometry in these cells to be $3HCO_3^-$:$1Na^+$ (Gross and Hopfer, 1996). Thus,

$$n = 1; \qquad m = 3 \tag{A12}$$

Equation A9 can then be rewritten as

$$i = 2FC\,\frac{\phi[\mathrm{Na}]_i[\mathrm{HCO_3}]_i^3 + \rho}{\sigma + \epsilon[\mathrm{HCO_3}]_i^3 + \gamma[\mathrm{Na}]_i + [\mathrm{Na}]_i[\mathrm{HCO_3}]_i^3} \tag{A13}$$

Under non-zero-trans conditions, the macro constants are

$$\phi = -(1/\mu)f_1^o f_2^o f_3 f_4 f_5 f_6 e^{-3\beta' u/2} \tag{A14}$$

$$\rho = (1/\mu)b_6b_1b_5b_2b_3b_4 \tag{A15}$$

$$\begin{aligned}\sigma = (1/\mu)(&b_6b_1b_2b_3b_4 + b_6b_1b_2b_3f_5 + b_6b_1b_2f_4f_5\\ &+ b_6b_1f_3f_4f_5\\ &+ b_1b_2b_3b_4b_6 + b_1b_2b_3f_5f_6 + b_1b_2f_4f_5f_6 + b_1f_3f_4f_5f_6\\ &+ b_6b_1b_2b_3b_5 + b_6b_1b_2f_4b_5 + b_6b_1f_3f_4b_5 + b_6b_1b_2b_4b_5\\ &+ b_6b_1f_3b_4b_5 + b_6b_1b_3b_4b_5 + b_6b_2b_3b_4b_5\\ &+ b_1b_2b_3b_4b_5)\end{aligned} \tag{A16}$$

$$\begin{aligned}\epsilon = (f_2^o/\mu)(&b_6f_3f_4f_5 + f_3f_4f_5f_6 + b_6f_3f_4b_5 + b_6f_3b_4b_5\\ &+ b_6b_3b_4b_5)e^{-3\beta' u/2}\end{aligned} \tag{A17}$$

$$\begin{aligned}\gamma = (f_1^o/\mu)(&b_2b_3b_4f_6 + b_2b_3f_5f_6 + b_2f_4f_5f_6 + f_3f_4f_5f_6\\ &+ b_2b_3b_4b_5)\end{aligned} \tag{A18}$$

$$\begin{aligned}\mu = f_1^o f_2^o(&f_3f_4f_5 + f_3f_4f_6 + f_3b_4f_6 + b_3b_4f_6 + f_3f_5f_6\\ &+ b_3f_5f_6 + f_4f_5f_6 + f_3f_4b_5 + f_3b_4b_5 + b_3b_4b_5)e^{-3\beta' u/2}\end{aligned} \tag{A19}$$

Under zero-trans conditions ($[Na^+]_o = 0$, $[Bic]_o = 0$, $b_4 = 0$, $b_5 = 0$), the macro constants reduce to

$$\phi = -(1/\mu)f_1^o f_2^o f_3 f_4 f_5 f_6 e^{-3\beta' u/2} \tag{A20}$$

$$\rho = 0 \tag{A21}$$

$$\sigma = (1/\mu)(b_6 + f_6)(b_2b_3 + b_2f_4 + f_3f_4)b_1f_5 \tag{A22}$$

$$\epsilon = (1/\mu)(f_2^o f_3 f_4 f_5)(b_6 + f_6)e^{-3\beta' u/2} \tag{A23}$$

$$\gamma = (1/\mu)f_1^o(b_2b_3 + b_2f_4 + f_3f_4)f_5f_6 \tag{A24}$$

$$\mu = f_1^o f_2^o(f_3f_4f_5 + f_3f_4f_6 + f_3f_5f_6 + b_3f_5f_6 + f_4f_5f_6)e^{-3\beta' u/2} \tag{A25}$$

In both cases the macro constants are independent of $[Na^+]_i$ and $[HCO_3^-]_i$.

Phenomenological current equations and constants

Under zero-trans conditions, the steady-state current equation (A13) can be rewritten in a phenomenological (Michaelis-Menten) form, as a function of either the intracellular Na^+ or HCO_3^- concentrations:

$$i = \frac{I_{max}^{Na}[\mathrm{Na}]_{in}}{K_{0.5}^{Na} + [\mathrm{Na}]_{in}} \tag{A26}$$

where

$$I_{max}^{Na} = 2FC_T\frac{\phi[\mathrm{HCO_3}]_{in}^3}{\gamma + [\mathrm{HCO_3}]_{in}^3} \tag{A27}$$

$$K_{0.5}^{Na} = \frac{\sigma + \epsilon[\mathrm{HCO_3}]_{in}^3}{\gamma + [\mathrm{HCO_3}]_{in}^3} \tag{A28}$$

or

$$i = \frac{I_{max}^{Bic}[\mathrm{HCO_3}]_{in}^3}{K_{0.5}^{Bic} + [\mathrm{HCO_3}]_{in}^3} \tag{A29}$$

$$I_{max}^{Bic} = 2FC_T\frac{\phi[\mathrm{Na}]_{in}}{\epsilon + [\mathrm{Na}]_{in}} \tag{A30}$$

$$K_{0.5}^{Bic} = \frac{\sigma + \gamma[\mathrm{Na}]_{in}}{\epsilon + [\mathrm{Na}]_{in}} \tag{A31}$$

The authors thank Mrs. Margaret Finesilver for her assistance with the cell cultures and Dr. Stephen Jones for helpful comments on the manuscript.

This work was supported by a grant-in-aid from the American Heart Association to EG, and National Institutes of Health grants HL41618 and DK07678 to UH.

REFERENCES

Acevedo, M. 1994. Effect of acetyl choline on ion transport in sheep tracheal epithelium. *Pflugers Arch.* 427:543–546.

Akiba, T., R. J. Alpern, J. Eveloff, J. Calamina, and D. G. Warnock. 1986. Electrogenic sodium/bicarbonate cotransport in rabbit renal cortical basolateral membrane vesicles. *J. Clin. Invest.* 78:1472–1478.

Alpern, R. J. 1985. Mechanism of basolateral membrane $H^+/OH^-/HCO_3^-$ transport in the rat proximal convoluted tubule. A sodium-coupled electrogenic process. *J. Gen. Physiol.* 86:613–636.

Alpern, R. J., and M. Chambers. 1986. Cell pH in the rat proximal convoluted tubule. Regulation by luminal and peritubular pH and sodium concentration. *J. Clin. Invest.* 78:502–510.

Backman, K., B. Harrison, M. Meysenberg, C. Schwartz, and W. Germann. 1992. Inactivation of a volume-sensitive basolateral potassium conductance in turtle colon: effect of metabolic inhibitors. *Biochim. Biophys. Acta.* 1105:89–96.

Bedlack, R. S., M.-d Wei, S. H. Fox, E. Gross, and L. M. Loew. 1994. Distinct electric potentials in soma and neurite membranes. *Neuron.* 13:1187–1193.

Bevington, P. R. 1969. Data Reduction and Error Analysis for the Physical Sciences. McGraw-Hill, New York. 314–315.

Biagi, B. A. 1985. Effect of the anion transport inhibitor, SITS, on the proximal straight tubule of the rabbit perfused in vitro. *J. Membr. Biol.* 88:25–31.

Biagi, B. A., and M. Sohtell. 1986. Electrophysiology of basolateral transport in the rabbit proximal tubule. *Am. J. Physiol.* 250:F267–F272.

Boron, W. F., and E. L. Boulpaep. 1983. Intracellular pH regulation in the renal proximal tubule of the salamander: basolateral HCO_3^- transport. *J. Gen. Physiol.* 81:53–94.

Burckhardt, B. C., K. Sato, and E. Fromter. 1984. Electrophysiological analysis of bicarbonate permeation across the peritubular cell membrane of rat kidney proximal tubule. I. Basic observation. *Pflugers Arch.* 401:34–42.

Burckhardt, B. C., P. Thelen, and G. Burckhardt. 1994. Expression of rat renal $Na^+HCO_3^-$ cotransporter in *Xenopus laevis* oocytes. *Pflügers Arch. Eur. J. Physiol.* 429:294–296.

Coppola, S., and E. Frömter. 1994. An electrophysiological study of angiotensin II regulation of Na-HCO_3 cotransport and K conductance in renal proximal tubules. II. Effect of micromolar concentrations. *Pflügers Arch.* 427:151–156.

Dorando, F. C., and R. K. Crane. 1984. Studies of the kinetics of Na^+-gradient-coupled glucose transport as found in brush-border membrane vesicles from rabbit jejunum. *Biochim. Biophys. Acta.* 772:273–287.

Emmett, M., R. J. Alpern, and D. W. Seldin. 1992. Metabolic acidosis. *In* The Kidney, Physiology and Pathophysiology. D. W. Seldin and G. Giebisch, editors. Raven Press Publishers, New York. 2759–2838.

Eyring, H., R. Lumry, and J. W. Woodbury. 1949. Some applications of modern rate theory to physiological systems. *Rec. Chem. Prog.* 10: 100–114.

Goldner, A. M., S. G. Schultz, and P. F. Curran. 1969. Sodium and sugar fluxes across the mucosal border of rabbit ileum. *J. Gen. Physiol.* 53:362–383.

Gross, E., R. S. Bedlack, and L. M. Loew. 1994. Dual-wavelength ratiometric measurement of the membrane dipole potential. *Biophys. J.* 67:208–216.

Gross, E., and U. Hopfer. 1996. Activity and stoichiometry of Na^+:HCO_3^- cotransport in immortalized renal proximal tubule cells. *J. Membr. Biol.* 152:245–252.

Hille, B. 1992. Ionic Channels of Excitable Membranes. Sinauer Associates, Sunderland, MA.

Hopfer, U., and R. Groseclose. 1980. The mechanism of Na^+-dependent D-glucose transport. *J. Biol. Chem.* 255:4453–4462.

Illek, B., H. Fischer, and W. Clauss. 1993. Quinidine sensitive K^+ channels in the basolateral membrane of embryonic coprodeum epithelium: regulation by aldosterone and thyroxine. *J. Comp. Physiol. B.* 163:556–562.

Jauch, P., and P. Läuger. 1986. Electrogenic properties of the sodium-alanine cotransporter in pancreatic acinar cells. II. Comparison with transport models. *J. Membr. Biol.* 94:117–127.

Jentsch, T. J., B. S. Schill, P. Schwartz, M. Matthes, S. K. Keller, and M. Wiederholt. 1985. Kidney epithelial cells of monkey origin (BSC-1) express a sodium bicarbonate cotransporter. *J. Biol. Chem.* 260: 15554–15560.

Jentsch, T. J., P. Schwartz, B. S. Schill, B. Langner, A. P. Lepple, S. K. Keller, and S. K. Wiederholt. 1986. Kinetic properties of the sodium bicarbonate (carbonate) symport in monkey kidney epithelial cells (BSC-1). *J. Biol. Chem.* 261:10673–10679.

Kessler, M., and G. Semenza. 1983. The small intestinal Na,D-glucose cotransporter: an assymetric gated channel (or pore) responsive to the membrane potential. *J. Membr. Biol.* 76:27–56.

Kimmich, G. A., and J. Randles. 1984. Sodium-sugar stoichiometry in chick intestinal cells. *Am. J. Physiol.* 247:C74–C82.

Kimmich, G. A., and J. Randles. 1988. Na-coupled sugar transport: membrane potential-dependent K_m and K_i for Na^+. *Am. J. Physiol.* 255: C486–C494.

King, E. L., and C. Altman. 1956. A schematic method of deriving the rate laws of enzyme-catalyzed reactions. *J. Phys. Chem.* 60:1375–1378.

Kirk, K. L., and D. C. Dawson. 1983. Basolateral potassium channel in turtle colon: evidence for single file flow. *J. Gen. Physiol.* 82:297–313.

Läuger, P. 1972. Carrier mediated ion transport. *Science.* 178:24–30.

Lopes, A. G., A. W. Siebens, G. Giebisch, and W. F. Boron. 1987. Electrogenic Na/HCO_3 cotransport across basolateral membrane of isolated perfused Necturus proximal tubule. *Am. J. Physiol.* 253:F340–F350.

Restrepo, D., and G. A. Kimmich. 1985. Kinetic analysis of mechanism of intestinal Na-dependent sugar transport. *Am. J. Physiol.* 248: C498–C509.

Romero, M. F., M. A. Hediger, E. L. Boulpaep, and W. F. Boron. 1997. Expression cloning and characterization of a renal electrogenic Na/HCO_3 cotransporter. *Nature.* 387:409–413.

Sanders, D. 1986. Generalized kinetic analysis of ion-driven cotransport systems. II. Random ligand binding as a simple explanation for non-Michaelis kinetics. *J. Membr. Biol.* 90:67–87.

Sanders, D., U. P. Hansen, D. Gradmann, and C. L. Slayman. 1984. Generalized kinetic analysis of ion driven cotransport systems: a unified interpretation of selective ionic effects on Michaelis parameters. *J. Membr. Biol.* 77:123–152.

Sasaki, S., T. Shiigai, and J. Takeuchi. 1985. Intracellular pH in the isolated perfused rabbit proximal straight tubule. *Am. J. Physiol.* 249: F417–F423.

Schultz, S. G. 1986. Ion-coupled transport of organic solutes across biological membranes. *In* Physiology of Membrane Disorders. T. E. Andreoli, J. F. Hoffman, D. D. Fanestil, and S. G. Schultz, editors. Plenum, New York. 283–294.

Schultz, S. G., and P. F. Curran. 1970. Coupled transport of sodium and organic solutes. *Physiol. Rev.* 50:637–718.

Segel, I. H. 1975. Enzyme Kinetics. John Wiley and Sons, New York.

Semenza, G. 1971. On the mechanism of mutual inhibition among sodium-dependent transport systems in the small intestine. A hypothesis. *Biochim. Biophys. Acta.* 241:637–649.

Soleimani, M., and P. S. Aronson. 1989. Ionic mechanism of Na^+:HCO_3^- cotransport in renal basolateral membrane vesicles. *J. Biol. Chem.* 264: 18302–18308.

Soleimani, M., S. M. Grassl, and P. S. Aronson. 1987. Stoichiometry of Na-HCO_3 cotransport in basolateral membrane vesicles isolated from rabbit renal cortex. *J. Clin. Invest.* 79:1276–1280.

Stein, W. D. 1984. Transport and Diffusion across Cell Membranes. Academic Press, San Diego. 520.

Stein, W. D. 1990. Channels, Carriers and Pumps. An Introduction to Membrane Transport. Academic Press, San Diego.

Stevens, B. R., J. D. Kaunitz, and E. M. Wright. 1984. Intestinal transport of amino acids and sugars: advances using membrane vesicles. *Annu. Rev. Physiol.* 46:417–433.

Umbach, J., M. J. Coady, and E. M. Wright. 1990. Intestinal Na/glucose cotransporter expressed in *Xenopus* oocytes is electrogenic. *Biophys. J.* 57:1218–1224.

Weirzbicki, W., A. Berteloot, and G. Roy. 1990. Pre-steady-state kinetics and carrier-mediated transport: a theoretical analysis. *J. Membr. Biol.* 117:11–27.

Woodbury, J. W. 1971. Eyring rate theory model of the current-voltage relationship of ion channels in excitable membranes. *In* Chemical Dynamics. J. O. Hirschfelder, editor. Wiley, New York. pp. 601–617.

Woost, P. G., D. E. Orosz, W. Jin, P. S. Frisa, J. W. Jacobberger, J. G. Douglas, and U. Hopfer. 1996. Immortalization and characterization of proximal tubule cells derived from kidneys of spontaneously hypertensive and normotensive rats. *Kidney Int.* 50:125–134.

Yoshitomi, K., B. C. Burckhardt, and E. Fromter. 1985. Rheogenic sodium-bicarbonate cotransport in the peritubular cell membrane of rat renal proximal tubule. *Pflügers Arch.* 405:360–366.

Yoshitomi, K., and E. Fromter. 1984. Cell pH of rat renal proximal tubule in vivo and the conductive nature of peritubular HCO_3^- exit. *Pflügers Arch.* 402:300–305.